1IL and 3MLCT excited states modulated by H+: structure and photophysical properties of [(2-bromo-5-(1H-pyrazol-1-yl)pyrazine)Re(CO)3Br]

N. Pizarro, M. Saldías, N. Guzmán, C. Sandoval-Altamirano, S. Kahlal, J.-Y. Saillard, J.-R. Hamon, A. Vega

1IL and 3MLCT excited states modulated by H+: structure and photophysical properties of [(2-bromo-5-(1H-pyrazol-1-yl)pyrazine)Re(CO)3Br]

N. Pizarro, M. Saldías, N. Guzmán, C. Sandoval-Altamirano, S. Kahlal, J.-Y. Saillard, J.-R. Hamon, A. Vega

^{1}IL and ^{3}MLCT Excited States Modulated by H^+: Structure and Photophysical Properties of [(2-bromo-5-(1H-pyrazol-1-yl)pyrazine)Re(CO)$_3$Br]

Nancy Pizarro,[a] Marianela Saldías,[a] Nicolás Guzmán,[a] Catalina Sandoval-Altamirano,[a] Samia Kahlal,[b] Jean-Yves Saillard,[b] Jean-René Hamon,[b] Andrés Vega*[a,c]

The reaction of 2-bromo-5-(1H-pyrazol-1-yl)pyrazine (**L$_I$**) and bromotricarbonyl(tetrahydrofuran)-rhenium(I) dimer leads to the monometallic complex [(2-bromo-5-(1H-pyrazol-1-yl)pyrazine)Re(CO)$_3$Br] (**I**), which displays a non-regular octahedral geometry around Re^I center, a *fac*-correlation for carbonyls, with pyrazine and pyrazolyl rings highly coplanar. **I** experiences one irreversible oxidation at $E_{p,a}$ = 1.067 V and two irreversible reductions at $E_{p,c}$ = -1.445 V and -1.675 V. DFT supports the oxidation is a metal-centered processes but the first reduction wave should be a ligand-centered process. Comparison with related complexes suggest the second reduction is metal centered (Re^I/Re^0). Three absorptions bands were observed for **I** around 260, 315 and 400 nm, the first two were assigned to intraligand (IL) $\pi \rightarrow \pi^*$ transitions while the band around 400 nm corresponds to a metal-to-ligand charge transfer (MLCT) transition. Excitation of **I** at 280 nm leads to two emission bands at 360 nm and 640 nm, the first one attributed to the ^{1}IL transition and the second to ^{3}MLCT. The ^{3}MLCT emission decays with lifetimes of 17 and 44 ns in MeCN and DCM, respectively. Addition of trifluoroacetic acid to the solution leads to its reaction with the ^{3}MLCT excited state, giving rise to a long-lived and very oxygen sensitive specie, ^{3}ILH$^+$. This behaviour makes **I** potential sensor for protons and possibly other cations in solution.

Introduction

Mononuclear rhenium(I) diimine tricarbonyl complexes have been recently subject of many investigations because of their interesting characteristics. This include well-behaved and general synthetic procedures, and, very importantly, remarkable stability.[1, 2] Uses and potential applications include light capture,[3-6] anion sensing,[7, 8] bio-labeling and therapy,[9-13] and carbon dioxide photo-reduction[4, 14-21] among others. Simple aromatic chelating di-imines, like phenanthroline or bipyridyl are appealing candidates to be explored; owing to their planarity and limited conformational flexibility; since they diminish non-radiative deactivation paths.[22, 23] Comparatively less studied, pyrazolyl-pyrazine derivatives are also attractive candidates having conjugated systems and structural rigidity. They are also relatively easy to prepare and to modify upon as request. Pyrazolyl-pyrazine ligands also offer, when coordinated, an additional nitrogen atom to act as an acid-base center, which would influence the photophysical properties of their complexes,[24, 25] adding an extra-feature to be considered for potential applications.

The literature shows pyrazolyl-pyridazine complexes of Fe^{II}, Co^{II} and Ru^{II}.[26-31] Transition metal complexes of 2,6-bis(pyrazol-1-yl)pyrazine derivatives have been described as tridentate and meridional ligands,[31] while complexes of mono-substituted pyrazine derivatives are scarce.[29, 32-34]

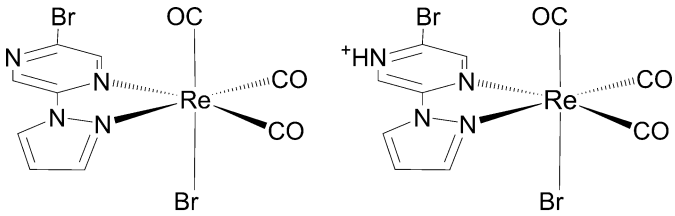

Scheme 1. Structural diagram of [(2-bromo-5-(1H-pyrazol-1-yl)pyrazine)Re(CO)$_3$Br] (**I**) and its protonated form **IH$^+$**.

To the best of our knowledge no previous example of a Re^I (d^6) complex has been reported with this kind of chelator. Then, expanding our research based on pyrazolyl-pyridazine derivatives,[35] in this work we extend the approach to the use of pyrazolyl-pyrazine as ligands. The synthesis and spectroscopic properties of the new rhenium(I) tricarbonyl complex (**I**) of the ligand 2-bromo-5-(1H-pyrazol-1-yl)pyrazine (**L$_I$**), shown in Scheme 1, are detailed. Density Functional Theory (DFT) and Time-Dependent DFT (TD-DFT) calculations have been used to

[a] *Universidad Andres Bello, Facultad de Ciencias Exactas, Departamento de Ciencias Químicas, Viña del Mar, Chile.*
[b] *Univ Rennes, CNRS, ISCR (Institut des Sciences Chimiques de Rennes) – UMR 6226, F-35000 Rennes, France.*
[c] *Centro para el Desarrollo de la Nanociencia y la Nanotecnología, CEDENNA.*
[d] *: Actual Address: Instituto de Investigación e Innovación en Salud, Facultad de Ciencias de la Salud, Universidad Central, Lord Cochrane 417, Santiago, Chile*
- The authors dedicate this article to the memory of our friend and colleague Prof. Jean-Yves Pivan, Ecole Nationale Supérieure de Chimie de Rennes, who recently passed away.
Electronic Supplementary Information (ESI) associated with this article can be found, in the online version, at http://dx.doi.org/xxxxx

rationalize these properties in terms of their electronic structures, in comparison with those of the uncoordinated ligand. The effect of acid on the photophysical properties is analyzed.

Experimental

General considerations.

All reagents were used as received from the supplier (Aldrich), with no purification before use. Solvents: dichloromethane (DCM, UvaSol® or SeccoSolv® grade, Merck), chloroform ($CHCl_3$, Analysis grade, EMSURE® Merck), acetonitrile (MeCN, Analysis grade, EMSURE® Merck), ethanol (EtOH, Analysis grade, EMSURE® Merck), methanol (MeOH, Analysis grade, EMSURE® Merck), N,N-dimethylformamide (DMF, Uvasol® grade, Merck), benzene (C_6H_6, Analysis grade, EMSURE® Merck), toluene ($C_6H_5CH_3$, Analysis grade, EMSURE® Merck), and trifluoroacetic acid (TFA, for synthesis, Merck) were employed as received. The ligand 2-bromo-5-(1H-pyrazol-1-yl)pyrazine ($\mathbf{L_I}$) was prepared according to the literature.[35] Standard Schlenk techniques were used for all manipulations.

Synthesis of [(2-bromo-5-(1H-pyrazol-1-yl)pyrazine)Re(CO)$_3$Br] (I). The complex was prepared following a previously described procedure,[23] by direct reaction of the ligand $\mathbf{L_I}$ (0.0557 g, 0.262 mmol) with bromotricarbonyl(tetrahydrofuran)-rhenium(I) dimer (Aldrich, 0.121 g, 0.133 mmol) at room temperature in dichloromethane solution (Scheme 2). Upon mixing, an orange solution was instantly obtained. Slow evaporation of the solvent at room temperature lead to yellow crystals of **I**. Crystalline material yield: 84%.

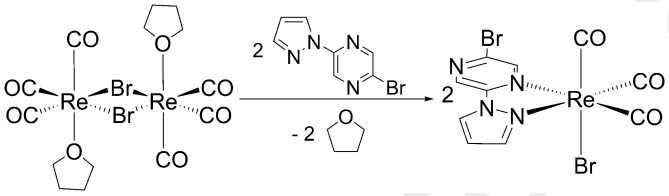

Scheme 2. Synthetic path to **I**.

Elemental Analysis: Flash 2000, Thermo Scientific, Organic elemental analyzer. Calculated (experimental) for $C_{10}H_5Br_2N_4O_3Re$: C, 20.9 (21.3); H, 0.88 (0.95); N, 9.74 (9.13) FTIR-ATR (major peaks cm^{-1}): $\nu_{C\equiv O}$: 2021, 1926, 1894; $\nu_{C=N}$: 1481, 1406 ν_{C-H}: 3146. ^{1}H NMR (400 MHz $(CD_3)_2SO$) δ(ppm) 9.60 (d, J = 0.9 Hz, 1H), 9.31 (d, J = 3.0 Hz, 2H), 9.15 (d, J = 0.9 Hz, 1H), 8.59 (s, 1H), 7.05 (d, J = 2.3 Hz, 1H), 7.04 (d, J = 2.2 Hz, 1H). ^{13}C NMR (101 MHz, $(CD_3)_2SO$) δ_C(ppm) 195.27, 186.6, 147.25, 146.24, 144.45, 136.60, 132.61, 112.51. (^{13}CNMR and ^{1}HNMR spectra in Fig. S1).

Structural determination. The crystal structure of **I** was determined by X-ray diffraction at 298 and, to check structural changes and dataset quality improvement, at 100 K, using a Bruker SMART-APEX II CCD diffractometer system. Data reduction was performed with SAINT.[36] Multi-scan absorption corrections were applied using SADABS.[37] The structure solution was by direct methods, completion by Difference Fourier Synthesis and refinement by least-squares using SHELXL.[38] The hydrogen atom positions were calculated after each cycle of refinement with SHELXL using a riding model, with a C—H distance of 0.96 Å. U_{iso}(H) values were set equal to $1.2U_{eq}$ of the parent carbon atom. Table S1 (prepared with Publcif [39]) shows a summary of structural and refinement details. No significant differences were found between the structures determined at 298 and 100 K.

Cyclic Voltammetry. Cyclic voltammograms at room temperature for $\mathbf{L_I}$ and **I** were recorded in a CH-INSTRUMENTS 650 E potentiostat in DMF solutions (1.0 mM) using tetrabuthylammonium perchlorate (0.10 M) as supporting electrolyte. Cyclic voltammograms were recorded at 100 mV s^{-1} between +1.7 and -1.7 V. Before runs, the sample solutions were deoxygenated by bubbling argon gas for 30 min. A vitreous carbon electrode was used as working electrode, a platinum electrode as auxiliary electrode, and an Ag/AgCl electrode as reference electrode. Ferrocene was used as internal standard ($E_{½}$ = 0.473 V vs Ag/AgCl, Ar); ΔE = 0.069 V (Ar)).

Spectroscopic and photophysical measurements. IR spectrum (4000-400 cm^{-1}) of the compound was measured using a Jasco FTIR-4600 spectrophotometer equipped with an ATR PRO ONE. ^{1}H and ^{13}C NMR spectra were recorded on a Bruker Avance 400 spectrometer at 298 K, using DMSO as solvent. UV-Vis spectra were recorded on an Agilent 8453 Diode-Array spectrophotometer in the range of 250-700 nm in aerated solvent solutions at room temperature. Emission spectra were measured in a Horiba Jobin-Yvon FluoroMax-4 spectrofluorometer in different solvents at room temperature or in ethanol-methanol glass (4:1, v/v) at 77 K. Luminescence lifetime measurements were carried out with the time correlated single photon counting technique using a PicoQuant FluoTime300 fluorescence lifetime spectrometer. A sub-nanosecond Pulsed Laser LDH-P-C-405 nm was employed as pulsed light sources (FWHM ~ 54 ps; average power 31 pJ). Time resolved experiments were made in different solutions, either air-equilibrated or argon-saturated. Emission quantum yields (Φ_{em}) were measured using procedures described in literature employing $[Ru(bpy)_3](PF_6)_2$ in acetonitrile solution as standard.[40] Singlet oxygen, $O_2(^1\Delta_g)$, measurements were carried out in a FluoTime 200 consisting in a multichannel scaler NanoHarp 200. Excitation at 355 nm was achieved with a pulsed laser (FTSS355-Q3, Crystal Laser, Berlin, Germany) working at 1 kHz repetition rate. For the detection of emission at 1270 nm a NIR PMT H10330A (Hamamatsu) was employed. The $O_2(^1\Delta_g)$ quantum yields (Φ_Δ) were determined by comparing the intensity at zero time of the 1270 nm signals to those of optically-matched solutions of phenalelone as reference (Φ_Δ = 0.95 in DCM).[41, 42] The transient difference absorption spectra and transient lifetimes were measured on an Edinburgh LP980 laser flash photolysis spectrometer. The excitation pump source was the Aurora II Integra 30 Nd:YAG/OPO system. The excitation wavelength was 355 nm (laser pulse ~ 10 mJ, 8.2 ns) for all the samples unless otherwise noted. For each measurement, optically dilute solutions were degassed by bubbling argon gas for about 20 min.

Computational Details. All geometry optimizations were performed by DFT calculations at the B3LYP/6-31+G(d,p)[43-46] level of theory using the Gaussian09 Rev C.01 package of programs (G09),[47] and started from geometry determined by

means of X-rays diffraction. The LANL2DZ basis set was used only for rhenium. The geometry optimization for **IH**$^{+}$ started at the one of **I**. The computations for the one electron oxidized **I**$^{+\bullet}$ or reduced **I**$^{-\bullet}$ species were done based on the optimized geometry for **I**. Excitation calculations were performed within the TD-DFT methodology as implemented in G09. Absorption and emission spectra were simulated from the above calculations using the GaussSum 3.0 suite of freely available processing tools. A full width at half-maximum (FWHM) of the Gaussian curves corresponding to 2000 cm^{-1} was employed to reproduce the spectra. Representations for molecular orbitals were generated using the G09 cubegen tool and have been visualized using VMD and Povray 3.6 programs.[48]

Results and discussion

Structural Description. Fig. 1 shows a molecular structure diagram for **I**. As clear from the figure, the coordination around Re^{I} is a distorted octahedron with facial carbonyl groups. Table 1 shows a summary of the main bond distances and angles. The pyrazolyl-pyrazine bite angle (N1-Re1-N3) is only 74.0(1)°, as required by the ligand. Both rings, pyrazine and pyrazolyl are nearly coplanar, as reflected by the N1-N2-C4-N3 torsion angle, -4.4(5)°.

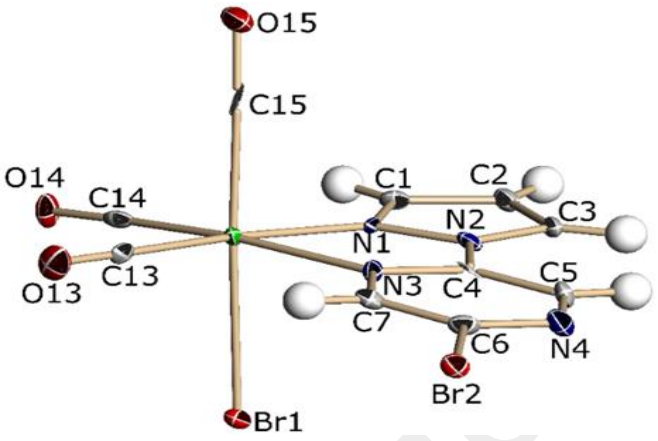

Fig. 1 Molecular structure diagram for **I** as determined at 100 K. Partial atom numbering is included. Displacement ellipsoids drawn at the 50% level of probability. Hydrogen atoms are drawn as spheres of arbitrary radii.

Table 1. Selected bond distances (Å) and angles (°) for **I** as determined by X-ray diffraction at 100 K.

Re1—C14	1.908(5)	Re1—N1	2.140(4)
Re1—C13	1.912(5)	Re1—N3	2.167(4)
Re1—C15	1.925(5)	Re1—Br1	2.5988(8)
C14—Re1—C13	86.77(19)	C15—Re1—N3	96.26(16)
C14—Re1—C15	89.93(18)	N1—Re1—N3	73.98(14)
C13—Re1—C15	91.65(18)	C14—Re1—Br1	89.06(13)
C14—Re1—N1	100.67(16)	C13—Re1—Br1	93.33(13)
C13—Re1—N1	172.34(16)	C15—Re1—Br1	174.84(12)
C15—Re1—N1	90.21(15)	N1—Re1—Br1	85.01(9)
C14—Re1—N3	171.78(15)	N3—Re1—Br1	84.30(9)
C13—Re1—N3	98.43(16)		

DFT, TD-DFT and Electronic Structure. To get a deeper insight into the electronic structure of this molecule, we performed DFT calculations by optimizing the gas phase geometry starting from the X-ray structure of **I**. As clear from Table S2, no important differences between the optimized and experimental distances are observed. Fig. 2 depicts the Kohn-Sham orbital diagram of **I**.

The optical transitions were computed by means of TD-DFT calculations assuming the DFT-optimized ground state geometry. Table 2 summarizes the energy of the major computed transitions, while Fig. 3 shows the simulated spectra of the molecule. The results are consistent with an absorption in the UV-Vis region of metal to ligand charge transfer (MLCT) nature.

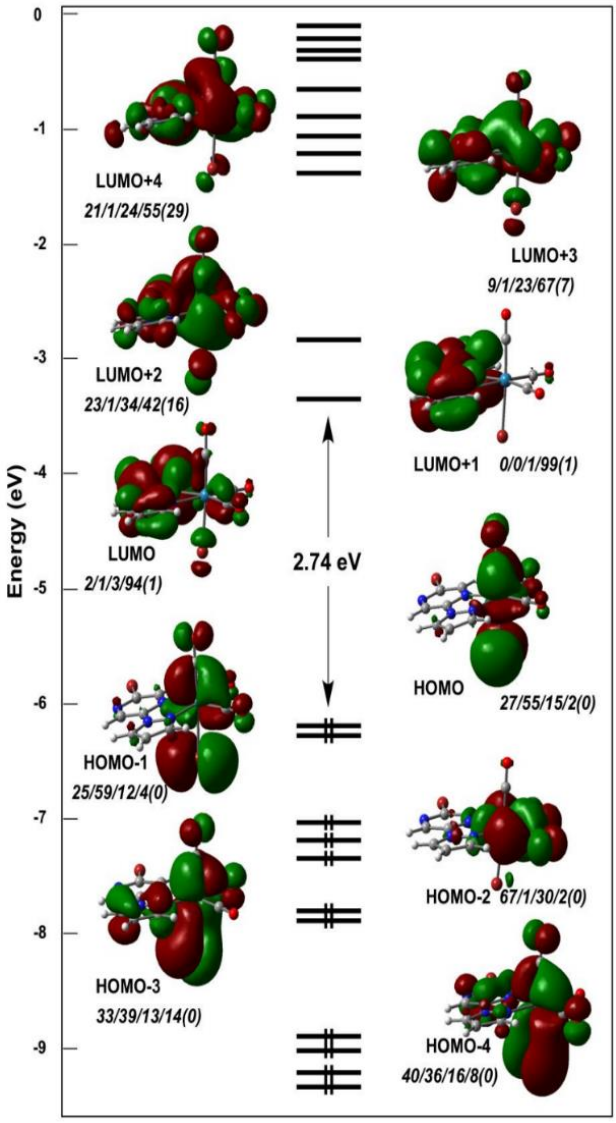

Fig. 2 Kohn-Sham orbital diagram computed for **I**, with the following % composition of: Re/Br(coordinated)/CO/**L**$_{I}$.

Table 2. Major TD-DFT-computed transitions for **I**, with their oscillator strength and associated charge transfer character.

λ / nm	*f*	Major Contributions	Character
368	0.085	HOMO-4 → LUMO (92 %)	$d\pi$(M+Br) → π^*(L$_I$)
306	0.132	HOMO-6 → LUMO (58 %)	π(L$_I$) → π^*(L$_I$)
269	0.284	HOMO-6 → LUMO+1 (78 %)	π(L$_I$) → π^*(L$_I$)

To study the protonation effect on the electronic structure of **I**, we have also performed DFT calculations for the protonated complex **IH**$^+$. Fig. S2. show frontier and near frontier Kohn-Sham orbitals for **IH**$^+$. For this specie the HOMO-LUMO transition has major $d\pi$(M+Br) $\rightarrow$ $d\pi^*$(M+Br+L_I) character. As shown in Fig. 2, the HOMO-LUMO GAP for **I** is computed to be 2.75 eV. The corresponding value for **IH**$^+$ diminishes to 1.60 eV. The same tendency is found for the difference in energy between ground state and the lowest energy triplet state, being 2.16 eV for **I** and 0.57 eV for **IH**$^+$.

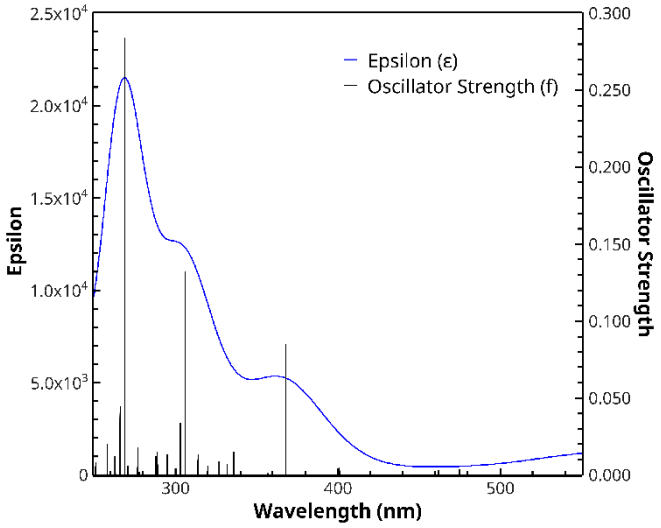

Fig. 3 TD-DFT computed spectrum for **I**, including oscillator strength for each transition.

Electrochemistry. To test the electrochemical behaviour and electronic structure of the ligand and the compound, we have carried out cyclic voltammetry experiments for both species in argon-saturated DMF solution. Table 3 shows a summary of the main cyclic voltammetry parameters. Under argon atmosphere, as expected, the positive scan reveals one irreversible oxidation for the complex around 1.1 V vs F_c^+/F_c, corresponding to Re^I/Re^{II} (Fig. 4, up), whose process is absent in the free ligand $\mathbf{L_I}$.

Table 3. Summary of cyclic voltammetry results for $\mathbf{L_I}$ and **I**. Potentials in V vs F_c^+/Fc in DMF with tetrabutylammonium perchlorate (0.1 M) as electrolyte.

	E_{p,c_1} (V)	E_{p,c_2} (V)	E_{p,c_3} (V)	E_{p,a_1} (V)
I	-1.445	-1.675	--	1.067
$\mathbf{L_I}$	--	--	-1.940	--

The negative scan displays a unique irreversible process for the ligand $\mathbf{L_I}$, a reduction wave with $E_{p,c}$ equal to -1.940 V (Fig. 4, below) while two irreversible reduction processes were observed for the complex at -1.445 V and -1.675 V. The first one is attributed to the reduction of the ligand by comparing with Re^I diimine ligands reported previously,[49, 50] while the second reduction wave at -1.675 V can be assigned to Re^I/Re^0 process such as has been observed in similar compounds of Re^I when dmf and dichloromethane solutions is used.[51, 52]

The assignment of redox processes on **I** is supported by the DFT computed spin density for the one-electron vertically oxidized or reduced species $\mathbf{I}^{\bullet+}$ and $\mathbf{I}^{\bullet-}$ (Fig. 5) and is consistent with metal centred oxidation and ligand centred reduction.

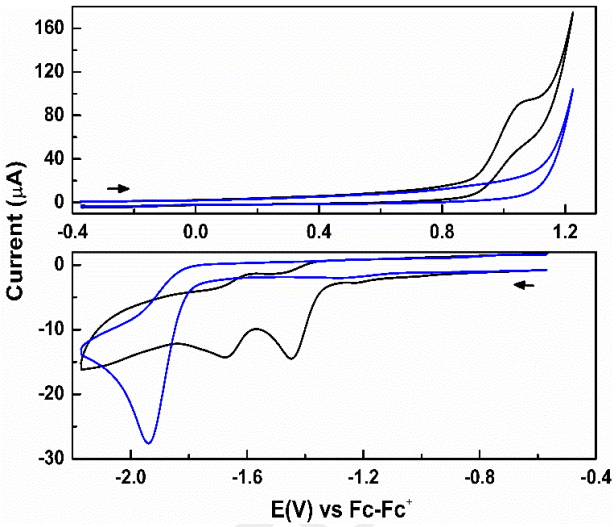

Fig. 4 Cyclic voltammograms for **I** (—) and $\mathbf{L_I}$ (—) measured in 1.0 mM argon saturated DMF solution. Tetrabutyl-ammonium perchlorate 0.10 M used as electrolyte.

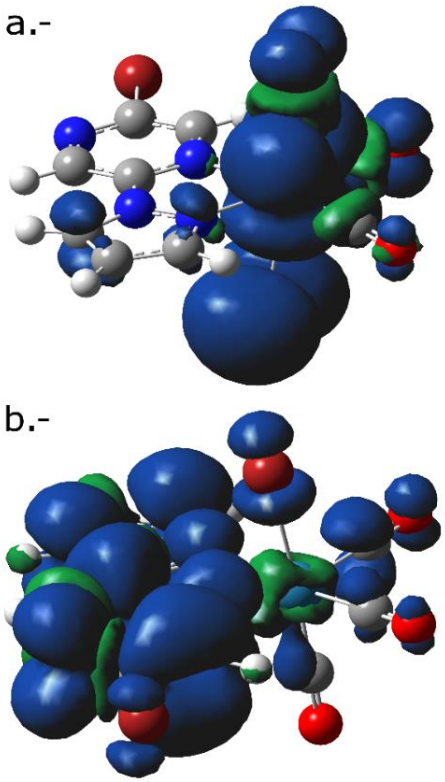

Fig. 5 DFT computed spin density for the one-electron vertically oxidized and reduced species $\mathbf{I}^{\bullet+}$ (a) and $\mathbf{I}^{\bullet-}$ (b).

It is important to note that the reductive behaviour of the rhenium complex is remarkably different from the free ligand, which has been described previously for a series of rhenium complexes with diazine ligands,[53] where it becomes clear that

coordination makes the ligand more electron poor and stabilizes the radical anion.

Absorption and emission properties. The absorption spectra for **I** and $\mathbf{L_I}$ in DCM and MeCN solutions are shown in Fig. 6. For **I,** three bands can be observed around 260, 315 and 400 nm. It is noteworthy that the computed and experimental spectra (Fig. 3) are in a satisfying agreement. The bands which are at shorter wavelengths display extinction coefficients in the order of 10^4 $M^{-1}cm^{-1}$ (Table 4). These two higher energy bands are also observed for the un-coordinated ligand ($\mathbf{L_I}$), being assigned to an intraligand $\pi \rightarrow \pi^*$ (IL) transitions. This agrees with the computed excitations, as shown in Table 2. On the other hand, the band centered at 400 nm has an extinction coefficient at least one order of magnitude lower and is consistent with the $d\pi(M+Br) \rightarrow \pi^*(L_I)$ charge transfer predicted by TD-DFT (Table 2). The hypsochromic shift of the longest wavelength band observed by changing the solvent from DCM to MeCN is consistent with the MLCT (more precisely MLLCT) assignation.

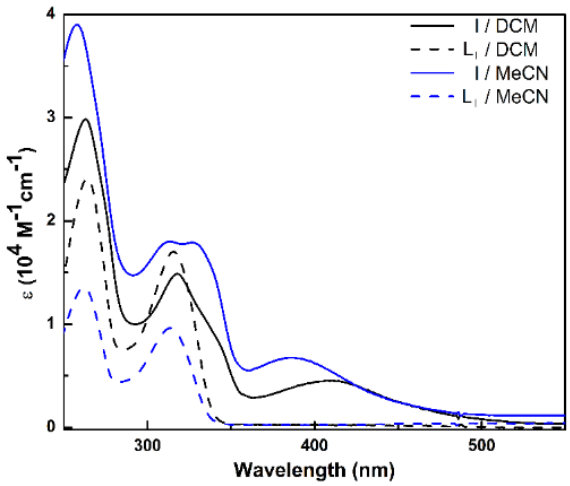

Fig. 6 Absorption spectra of **I** (solid lines) and $\mathbf{L_I}$ (dashed lines) in aerated DCM and MeCN solutions.

Fig. 7a and 7b show the emission spectra measured in aerated MeCN and DCM solutions for **I** upon excitation at 280 nm. Two emission bands around 360 nm and 640 nm can be observed. The broad emission at longer wavelength is assigned to an MLCT excited state, while the higher energy band is similar in energy to the uncoordinated ligand ($\mathbf{L_I}$) and is attributed to the $\pi_{pyrazine} \rightarrow \pi^*_{pyrazine}$ IL transition.[35] The second emission band of L_I (~430 nm, shoulder in the case of MeCN) is not observed when coordination to the metal takes place. The lower energy emission of the ligand could be related to a $\pi_{pyrazol} \rightarrow \pi^*_{pyrazine}$ IL transition or to the presence of a twisted intramolecular charge transfer (TICT) excited state.[54] These transitions would not be expected following coordination. Emission lifetimes at the higher energy emission bands of **I** were also coincident with the reported ones for the free ligand (see Table 4, and following sentences).[35]

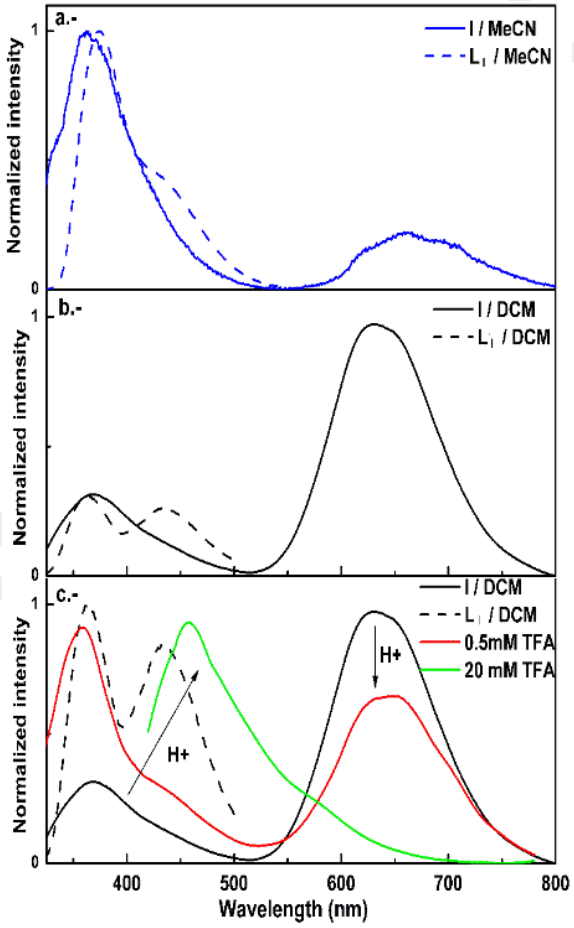

Fig. 7 Emission spectra of **I** in: **a**, MeCN, **b**, DCM and **c**, adding TFA to aerated DCM solution (λ_{exc} 280 nm). $\mathbf{L_I}$ spectrum was added[35] (dashed lines) for comparison.

Table 4. Summary of photophysical properties measured for $\mathbf{L_I}$ and **I** in solution of DCM and MeCN.

Compound	Solvent	λ_{abs} / nm (ε / 10^4 $M^{-1}cm^{-1}$)	λ_{em}/nm	$\Phi_{em, air}$	$\Phi_{em, Ar}$	τ_{air} / ns	τ_{Ar} / ns	$k_{r, Ar}$ / 10^6 s^{-1}	Φ_Δ
L_I	DCM	262 (1.4) 314 (1.0)	360, 440[a]	0.0100[a]	0.0230[a]	1.4 6.7	1.9	12.1	0.09
	MeCN	264 (2.4) 316 (1.7)	372, 432[a]	0.0250[a]	0.0480[a]	1.8 8.4	1.2 5.5	40.0 8.73	0.11
I	DCM	263 (3.0) 317 (1.4) 409 (0.5)	371[b] 645[b]	- 0.0016[c]	- 0.0018[c]	- 44.0[c]	- 49.0[c]	0.037	0.09
	MeCN	258 (3.9) 313 (1.8) 386 (0.7)	364[b] 630[b]	- 0.0006[c]	- 0.0014[c]	- 17.0[c]	- 20.2[c]	0.070	0.08

Errors were lower than 10%. [a] λ_{ex} = 280 nm. [b] λ_{ex} = 280 or 405 nm. [c] λ_{ex} = 405 nm. For **I**, Φ_{em} and τ were evaluated at 645 nm. λ_{ex} = 355 nm for Φ_Δ.

However, when trifluoroacetic acid (TFA) is added to **I** in air-equilibrated DCM solution, an increase of the emission intensity at 470 nm is observed (Fig. 7c), while the intensity at 645 nm decreases. It must be stated that after protonation, the absorption spectrum of complex **I** remains unchanged (see Fig. S3 in supplementary material), which would be an evidence of an excited-state reaction. Then, just the excited state seems to be modulated when acid is added to the medium. Since the excited state has MLLCT character, it might be protonated even though the ground state it is not (the electron density on the ligand is increased).

The characteristic rigidochromic effect of the emissive MLCT excited state for **I** is confirmed by the emission spectrum at 77 K in EtOH:MeOH (4:1) shown in Fig. 8.[55] A structureless band centered at 570 nm is observed with higher intensity when compared with emission at 298 K. The weak emission displayed for **I** at room temperature in the mixture of polar protic solvents is centered around 450 nm, which agrees with a favored emission from the IL excited state for the **IH**$^+$ specie.

Time resolved emission experiments allow us to observe a single exponential luminescence decay at 645 nm upon excitation at 405 nm in aerated MeCN and DCM solutions for **I** (Fig. 9), with lifetimes of 17 and 44 ns, respectively. This emission is associated to the MLCT excited state, while at higher energy (~470 nm), a biexponential emission decay is observed, which can be related to the IL singlet excited states with lifetimes similar to the reported ones for the non-coordinated ligand $\mathbf{L_I}$.[35]

Even though the emission quantum yields (Φ_{em}) and lifetimes (τ) were almost not affected by the presence of oxygen, a triplet character can be attributed to the emissive MLCT excited state due to the ultrafast intersystem crossing that has been reported for this kind of complexes.[56, 57] Moreover, a notable difference can be observed between the radiative rate constants (k_r) reported in Table 4, for the emission with IL or MLCT character, with the IL emission k_r being two orders of magnitude larger. The generation of singlet oxygen, $O_2(^1\Delta_g)$, was detected following the emission at 1270 nm upon excitation of aerated solutions. The singlet oxygen quantum yields (Φ_Δ) are included in Table 4. Values were comparable to the reported ones for similar complexes.[58] However, due to the similarity of Φ_Δ with the reported values for the free ligand,[35] it is also possible that singlet oxygen is being sensitized by an IL triplet excited state, then the ^{3}IL excited state must be close in energy to MLCT. Nevertheless, we have no additional data to prove that the triplet IL plays a significant role in the excited state behaviour.

The MLCT excited state is dynamically quenched after the addition of TFA to the aerated DCM solutions. As shown in Fig. 10, the emission lifetime at 645 nm (τ = 44 ns) is reduced after the addition of acid (τ = 7 ns at 0.0218 M TFA), with a quenching rate constant k_q equal to 5.5 x 10^9 M^{-1} s^{-1} (see Stern-Volmer plot in supplementary material, Fig. S4). The protonated excited state or the specie **IH**$^+$ favored the emission from the IL excited state at 470 nm. The time resolved emission spectra (TRES, inset in Fig. 10) shows that the biexponential decay has two components: τ_1 = 1.72 ns and τ_2 = 6.89 ns, which are coincident with the reported lifetimes for the transition with IL character of the non-coordinated ligand.[35] Absorption spectral changes must occur if the ground state energy is affected upon protonation, as previously reported for other complexes.[59]

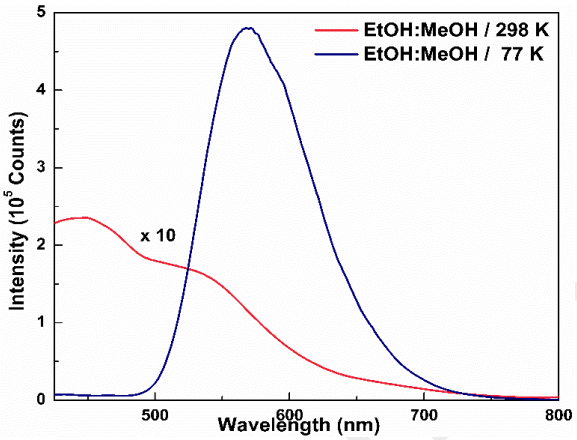

Fig. 8. Emission spectra of **I** in EtOH:MeOH 4:1 at 77 K and 298 K (λ_{ex} = 400 nm).

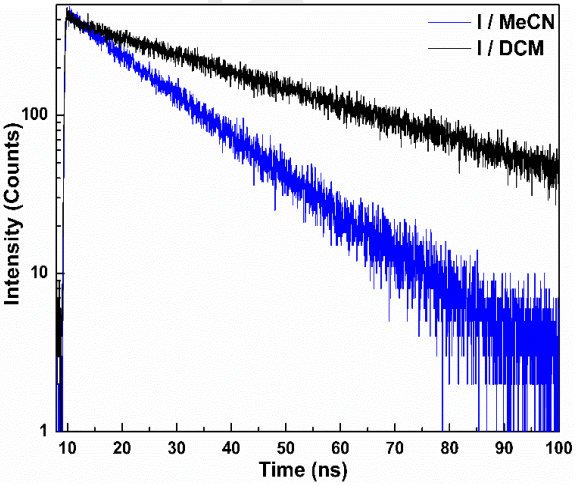

Fig. 9 Single exponential emission decays for **I** in aerated MeCN and DCM solutions (λ_{em} = 645 nm and λ_{ex} = 405 nm).

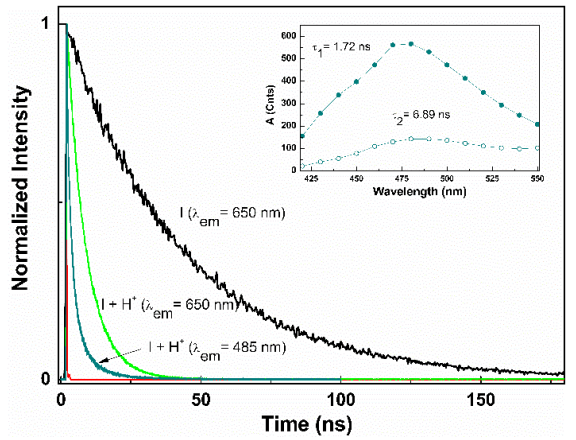

Fig. 10 Emission decay for **I** in aerated DCM solution with and without TFA (λ_{em} 485 or 650 nm and λ_{ex} = 405 nm). ***Inset:*** TRES of **I** upon addition of TFA in aerated DCM solution. For clarity, we just include the higher energy region (420 nm to 550 nm).

The transient absorption spectrum for **I** in deaerated DCM solution upon excitation at 355 nm is displayed in Fig. 11. The maximum of the transient absorption at 520 nm decays single exponentially with a lifetime τ = 50.8 ns, which can be related to the ^{3}MLCT excited state. Upon TFA addition in absence of oxygen, the maximum in the transient absorption spectrum displayed a hypsochromic shift to 460 nm, being comparable with the transient absorption band previously reported for the pyrazolyl-pyrazine ligand.[35] The trace decay is now biexponential with two lifetimes: the short component, τ = 49 ns, and the long component, τ_{T2} = 2.50 μs. The longer lifetime is coincident with the value reported for the ^{3}IL excited state of a similar ligand to L_I.[35] While the transient absorption for **I** is still displayed in aerated solutions, it was not possible to observe the transient absorption in aerated solution upon TFA addition. Then, the transition with IL character is more sensible to the presence of oxygen and the long-lived triplet of the protonated species seems to sensitize oxygen readily.

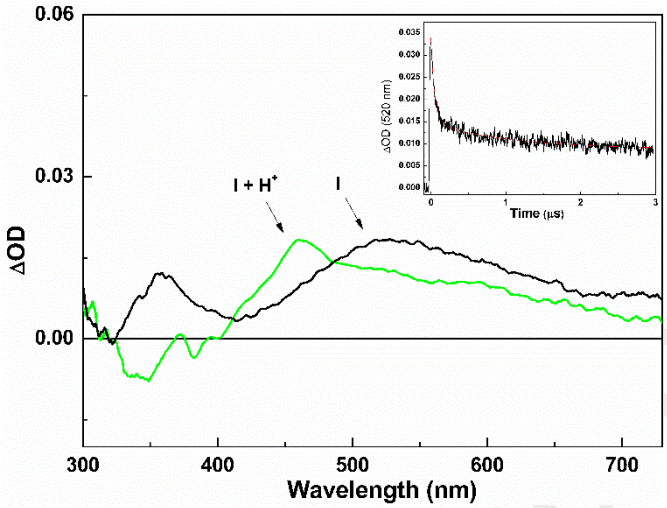

Fig. 11 Transient absorption spectra of **I** in deaerated DCM solution, in absence (black line) and in presence of TFA (green line), at room temperature and 140 ns after excitation at 355 nm. Inset shows the trace decay at 520 nm upon addition of acid in deaerated DCM solution.

Considering the results, we were able to propose the reaction sequence diagram shown in Scheme 3.

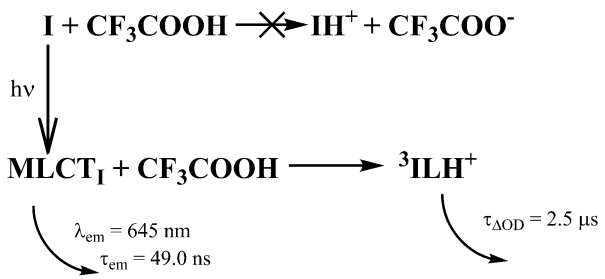

Scheme 3. Summary of the emissive behavior of each specie present in solution upon the addition of trifluoroacetic acid to a DCM solution of **I**.

The emission bands observed for **I** at higher energy can be ascribed to a singlet excited state with ^{1}IL character, while the one at lower energy is assigned to a triplet ^{3}MLCT excited state. We hypothesize that the trifluoroacetic acid addition to the medium do not produce the **IH$^+$** specie. In contrast the ^{3}MLCT excited state may react with the acid to sensitize the IL excited state of the protonated specie (^{3}ILH$^+$), a long-lived triplet excited state which is very sensitive to the oxygen presence in solution.

Conclusions

The monometallic complex [(2-bromo-5-(1H-pyrazol-1-yl)pyrazine)Re(CO)$_3$Br] (**I**), can be easily synthesized from the reaction of 2-bromo-5-(1H-pyrazol-1-yl)pyrazine (**L_I**) and bromotricarbonyl(tetrahydrofuran)-rhenium(I) dimer. **I** display a non-regular octahedral geometry around Re^I center, a *fac*-correlation for carbonyls, with pyrazine and pyrazolyl rings highly coplanar. Voltammetry experiments and theoretical DFT calculations support the oxidation is metal-centered processes and the first reduction is ligand centered. Absorption bands were assigned to intraligand $\pi \rightarrow \pi^*$ transitions and metal-to-ligand charge transfer transition. Excitation of **I** at 280 nm leads to two emission bands, the first one associated to the singlet IL excited state (^{1}IL), while the second one to the triplet MLCT excited state (^{3}MLCT). The ^{3}MLCT lifetime was sensible to the solvent polarity. The trifluoroacetic acid, when added to the solution, may react with the ^{3}MLCT excited state yielding the long-lived and oxygen sensitive state ^{3}ILH$^+$. These findings make **I** a potential sensor for protons and possibly other cations.

Conflicts of interest

Authors have no interest conflicts to declare.

Acknowledgements

The authors gratefully acknowledge partial financial support of Comisión Nacional Científica y Tecnológica, grants FONDECYT 1160546, 1160749, FONDEQUIP EQM 160099, ACT-1404 (IPMaG). AV acknowledges Financiamiento Basal para Centros Científicos y Tecnológicos de Excelencia FB0807. This research has been performed as part of the Chilean-French International Associated Laboratory for "Multifunctional Molecules and Materials" (LIA M3 - CNRS N°1207).

Notes and References

‡ CCDC-1575690 and CCDC-1581005 contains the supplementary crystallographic data for **I** measured at 296 and 100 K respectively. These data can be obtained free of charge via http://www.ccdc.cam.ac.uk/conts/retrieving.html, or from the Cambridge Crystallographic Data Centre, 12 Union Road, Cambridge CB2 1EZ, UK; fax: (+44) 1223-336-033; or e-mail: deposit@ccdc.cam.ac.uk.

1. D. J. Stufkens, *Comments on Inorganic Chemistry*, 1992, **13**, 359-385.

2. A. Kumar, S.-S. Sun and A. J. Lees, in *Photophysics of Organometallics*, ed. A. J. Lees, Springer: Berlin Heidelberg, 2010, DOI: 10.1007/3418_2009_2, pp. 37-71.
3. L. M. Kiefer, J. T. King and K. J. Kubarych, *Acc. Chem. Res.*, 2015, **48**, 1123-1130.
4. S. Sato, T. Arai and T. Morikawa, *Inorg. Chem.*, 2015, **54**, 5105-5113.
5. T. A. Oriskovich, P. S. White and H. H. Thorp, *Inorg. Chem.*, 1995, **34**, 1629-1631.
6. K. K. Lo, M. W. Louie, K. S. Sze and J. S. Lau, *Inorg. Chem.*, 2008, **47**, 602-611.
7. K.-C. Chang, S.-S. Sun, M. O. Odago and A. J. Lees, *Coord. Chem. Rev.*, 2015, **284**, 111-123.
8. K. C. Chang, S. S. Sun and A. J. Lees, *Inorg. Chim. Acta*, 2012, **389**, 16-28.
9. M. Salmain, M. Gunn, A. Gorfti, S. Top and G. Jaouen, *Bioconjugate Chem.*, 1993, **4**, 425-433.
10. G. Santoro, T. Zlateva, A. Ruggi, L. Quaroni and F. Zobi, *Dalton Trans.*, 2015, **44**, 6999-7008.
11. K. Wahler, A. Ludewig, P. Szabo, K. Harms and E. Meggers, *Eur. J. Inorg. Chem.*, 2014, **2014**, 807-811.
12. D. L. Ma, C. M. Che, F. M. Siu, M. Yang and K. Y. Wong, *Inorg. Chem.*, 2007, **46**, 740-749.
13. M. W. Louie, A. W. T. Choi, H. W. Liu, B. T. N. Chan and K. K. W. Lo, *Organometallics*, 2012, **31**, 5844-5855.
14. C. D. Windle, M. V. Campian, A. K. Duhme-Klair, E. A. Gibson, R. N. Perutz and J. Schneider, *Chem. Commun.*, 2012, **48**, 8189-8191.
15. C. D. Windle, E. Pastor, A. Reynal, A. C. Whitwood, Y. Vaynzof, J. R. Durrant, R. N. Perutz and E. Reisner, *Chem. Eur. J.*, 2015, **21**, 3746-3754.
16. T. W. Schneider and A. M. Angeles-Boza, *Dalton Trans.*, 2015, **44**, 8784-8787.
17. F. Franco, C. Cometto, C. Garino, C. Minero, F. Sordello, C. Nervi and R. Gobetto, *Eur. J. Inorg. Chem.*, 2015, DOI: 10.1002/ejic.201402912, 296-304.
18. G. Sahara and O. Ishitani, *Inorg. Chem.*, 2015, **54**, 5096-5104.
19. J. Agarwal, E. Fujita, H. F. Schaefer, 3rd and J. T. Muckerman, *J. Am. Chem. Soc.*, 2012, **134**, 5180-5186.
20. T. Morimoto, T. Nakajima, S. Sawa, R. Nakanishi, D. Imori and O. Ishitani, *J. Am. Chem. Soc.*, 2013, **135**, 16825-16828.
21. J. Shakeri, H. Hadadzadeh and H. Tavakol, *Polyhedron*, 2014, **78**, 112-122.
22. N. Pizarro, M. Duque, E. Chamorro, S. Nonell, J. Manzur, J. R. de la Fuente, G. Gunther, M. Cepeda-Plaza and A. Vega, *J. Phys. Chem. A*, 2015, **119**, 3929-3935.
23. F. Venegas, N. Pizarro and A. Vega, *J. Chil. Chem. Soc.*, 2011, **56**, 823-826.
24. K. Ranasinghe, S. Handunnetti, I. C. Perera and T. Perera, *Chem. Cent. J.*, 2016, **10**, 71.
25. M. Haga, E. S. Dodsworth, G. Eryavec, P. Seymour and A. B. P. Lever, *Inorg. Chem.*, 1985, **24**, 1901-1906.
26. G. Juhász, R. Matsuda, S. Kanegawa, K. Inoue, O. Sato and K. Yoshizawa, *J. Am. Chem. Soc.*, 2009, **131**, 4560-4561.
27. V. A. Money, J. Elhaik, I. Radosavljevic Evans, M. A. Halcrow and J. A. K. Howard, *Dalton Trans.*, 2004, DOI: 10.1039/B311262B, 65-69.
28. M. L. Soriano, F. A. Jalón, B. R. Manzano and M. Maestro, *Inorg. Chim. Acta*, 2009, **362**, 4486-4492.
29. G. Gupta, S. Gloria, B. Das and K. M. Rao, *J. Mol. Struct.*, 2010, **979**, 205-213.
30. C. A. Kilner and M. A. Halcrow, *Polyhedron*, 2006, **25**, 235-240.
31. R. Mohammed, G. Chastanet, F. Tuna, T. L. Malkin, S. A. Barrett, C. A. Kilner, J.-F. Létard and M. A. Halcrow, *Eur. J. Inorg. Chem.*, 2013, **2013**, 819-831.
32. L. Y. Yang and J. M. Shi, *Acta Crystallogr. E*, 2008, **64**, m1387.
33. S. Sangilipandi, D. Sutradhar, K. Bhattacharjee, W. Kaminsky, S. R. Joshi, A. K. Chandra and K. Mohan Rao, *Inorg. Chim. Acta*, 2016, **441**, 95-108.
34. M. Loï, M. W. Hosseini, A. Jouaiti, A. De Cian and J. Fischer, *Eur. J. Inorg. Chem.*, 1999, **1999**, 1981-1985.
35. N. Pizarro, G. Prado, M. Saldias, C. Sandoval-Altamirano and A. Vega, *Photochem. Photobiol.*, 2018, DOI: 10.1111/php.12911.
36. M. SAINTPLUS V6.22 Bruker AXS Inc., WI, USA., *Journal*.
37. W. SADABS V2.05 Bruker AXS Inc. Madison, USA., *Journal*.
38. G. M. Sheldrick, *Acta Crystallogr. A*, 2008, **64**, 112-122.
39. S. Westrip, *J. Appl. Crystallogr.*, 2010, **43**, 920-925.
40. K. Suzuki, A. Kobayashi, S. Kaneko, K. Takehira, T. Yoshihara, H. Ishida, Y. Shiina, S. Oishi and S. Tobita, *Phys. Chem. Chem. Phys.*, 2009, **11**, 9850-9860.
41. F. Wilkinson, W. P. Helman and A. B. Ross, *J. Phys. Chem. Ref. Data*, 1993, **22**, 113-262.
42. R. Schmidt, C. Tanielian, R. Dunsbach and C. Wolff, *J. Photochem. Photobiol. A*, 1994, **79**, 11-17.
43. P. J. Stephens, F. J. Devlin, C. F. Chabalowski and M. J. Frisch, *J. Phys. Chem.*, 1994, **98**, 11623-11627.
44. A. D. Becke, *J. Chem. Phys.*, 1993, **98**, 5648-5652.
45. S. H. Vosko, L. Wilk and M. Nusair, *Can. J. Phys.*, 1980, **58**, 1200-1211.
46. C. Lee, W. Yang and R. G. Parr, *Phys. Rev. B*, 1988, **37**, 785-789.
47. M. J. T. Frisch, G. W.; Schlegel, H. B.; Scuseria, G. E.; Robb, M. A.; Cheeseman, J. R.; Scalmani, G.; Barone, V.; Mennucci, B.; Petersson, G. A.; Nakatsuji, H.; Caricato, M. et al., *Gaussian 09*, Gaussian, Inc., 2009.
48. W. Humphrey, A. Dalke and K. Schulten, *J. Mol. Graph.*, 1996, **14**, 33-38.
49. M.-W. Louie, H.-W. Liu, M. H.-C. Lam, T.-C. Lau and K. K.-W. Lo, *Organometallics*, 2009, **28**, 4297-4307.
50. H. Y. V. Ching, X. Wang, M. He, N. Perujo Holland, R. Guillot, C. Slim, S. Griveau, H. C. Bertrand, C. Policar, F. Bedioui and M. Fontecave, *Inorganic Chemistry*, 2017, **56**, 2966-2976.
51. C. Bruckmeier, M. W. Lehenmeier, R. Reithmeier, B. Rieger, J. Herranz and C. Kavakli, *Dalton Transactions*, 2012, **41**, 5026-5037.
52. J. C. Canales, A. Carreño, D. Oyarzún, J. M. Manríquez and I. Chávez, *J. Chil. Chem. Soc*, 2018, **62**, 3765-3771.
53. M. Panigati, M. Mauro, D. Donghi, P. Mercandelli, P. Mussini, L. De Cola and G. D'Alfonso, *Coord. Chem. Rev.*, 2012, **256**, 1621-1643.
54. S. Sasaki, G. P. C. Drummen and G.-i. Konishi, *J. Mater. Chem. C*, 2016, **4**, 2731-2743.
55. A. J. Lees, *Comments on Inorganic Chemistry*, 1995, **17**, 319-346.
56. A. El Nahhas, A. Cannizzo, F. van Mourik, A. M. Blanco-Rodríguez, S. Záliš, A. Vlček and M. Chergui, *J. Phys. Chem. A*, 2010, **114**, 6361-6369.
57. A. El Nahhas, C. Consani, A. M. Blanco-Rodríguez, K. M. Lancaster, O. Braem, A. Cannizzo, M. Towrie, I. P. Clark, S.

Záliš, M. Chergui and A. Vlček, *Inorganic Chemistry*, 2011, **50**, 2932-2943.
58. F. Ragone, P. D. Gara, F. S. García Einschlag, A. G. Lappin, G. J. Ferraudi, E. Wolcan and G. T. Ruiz, *Journal of Photochemistry and Photobiology A: Chemistry*, 2018, **358**, 147-156.
59. H. Xue, W. Li-Zhu, S. Gang, P. Jie, Y. Qing-Zheng, Z. Li-Ping and T. Chen-Ho, *Chem. Eur. J.*, 2007, **13**, 1231-1239.